Influence of Dopant Elements on Degradation Phenomena in B- and Ga-Doped Czochralski-Grown Silicon

Wolfram Kwapil,* Jonas Dalke, Regina Post, and Tim Niewelt

The response of lifetime samples made from boron- and gallium-doped Czochralski-grown silicon from the same producer to light- and elevated temperature-induced degradation (LeTID) conditions (varying illumination at 75 °C), to dark anneals (DAs) at 175 °C, and the temporary recovery (TR) reaction under different conditions is investigated. It is found that Ga-doped samples behave very differently than their B-doped counterparts: while the carrier lifetime remains at a high level if an illumination equivalent to 1 sun at 75 °C is applied, strong carrier lifetime degradation occurs at low light intensities. A capture cross-sectional ratio in degraded Ga-doped samples of ~26 is found, which is typical for the LeTID defect. TR of this degraded state is observed on Ga-doped samples when the illumination intensity is increased at 75 °C and when samples are illuminated at 25 °C with intermediate intensity. During DA of B-doped samples, a bulk-related degradation and a subsequent surface-related degradation are observed. In contrast, degradation of Ga-doped samples during DA only occurs on long timescales, and its cause is not clear, yet. It is concluded that the specific dopant species plays an active role both during LeTID and for surface-related degradation—possibly as a result of differences in the acceptor–hydrogen pair properties.

1. Introduction

Having dominated the photovoltaic industry for more than 20 years, the use of boron as a doping agent of the silicon wafers is currently on the retreat. The main reason for this transformation is the deleterious impact of the boron–oxygen (BO) defect in industrial Czochralski-grown (Cz) silicon wafers. The presence of this defect causes significant reduction of charge carrier lifetime and, thereby, solar cell performance upon illumination termed light-induced degradation (LID) at normal ambient temperature.[1,2] This effect can be mitigated by additional process steps[3] at additional cost. As Ga-doped silicon wafers are not affected by BO defects, they do not exhibit BO-LID.[4] Therefore, Ga-doped Cz silicon seems to be an attractive alternative, allowing for high cell efficiency without additional process steps.

A second degradation effect appearing under light and elevated temperature-induced degradation (LeTID) has attracted attention in the past years due to its detrimental influence especially on passivated emitter and rear contact (PERC) solar cells. Contrary to BO-LID, LeTID has been detected in many different materials, such as boron- or phosphorus-doped Cz silicon,[5–7] quasimono-crystalline silicon,[8] multicrystalline (mc) silicon,[9,10] and float-zone (FZ) silicon.[11,12] It is general consensus that the introduction of hydrogen into the wafer plays a significant role in the LeTID degradation.[6,12–15] Therefore, high-temperature process steps allowing the release of hydrogen from dielectric layers seem to be key to controlling LeTID.[16–19]

It has been shown early on that the Ga-doped wafers and solar cells exhibit a similar degradation at elevated temperature as B-doped counterparts.[9] There seem to exist some differences: in Ga-doped mc-Si, LeTID proceeds at a lower rate than in B-doped mc-Si,[20] and the degradation extent of Ga-doped Cz-Si at typical LeTID conditions (75 °C, illumination of 1 sun equivalent) was shown to be lower than in B-doped Cz-Si in some cases,[21] whereas significant degradation was observed in others.[22] However, in these studies, differences in the crystalline structure or the processing conditions could have interfered with the LeTID effect, making it difficult to attribute differences to the dopants.

A third degradation phenomenon is the deterioration of surface passivation on long timescales under field operation conditions. The stability has been shown to depend significantly on the type of passivation stack. Single SiN_x layers are highly sensitive to illumination at elevated temperatures,[23] whereas an interlayer of either AlO_x or SiO_x slows down the degradation reaction.[24–26] In addition, it was demonstrated that a highly doped silicon surface region (emitter) underneath the passivation stack leads to a significantly increased stability of the surface

Dr. W. Kwapil, R. Post, Dr. T. Niewelt
Laboratory for Photovoltaic Energy Conversion
Department of Sustainable Systems Engineering (INATECH)
University of Freiburg
Emmy-Noether-Str. 2, 79110 Freiburg, Germany
E-mail: wolfram.kwapil@ise.fraunhofer.de

Dr. W. Kwapil, J. Dalke, R. Post, Dr. T. Niewelt
Division Photovoltaics
Department Quality Assurance, Characterization, and Simulation
Fraunhofer Institute for Solar Energy Systems (ISE)
Heidenhofstraße 2, 79110 Freiburg, Germany

ⓘ The ORCID identification number(s) for the author(s) of this article can be found under https://doi.org/10.1002/solr.202100147.

passivation.[27,28] Although not investigated thoroughly, it is likely that the influence of the surface doping layers can be attributed to the influence of the electric fields as a result of the doping gradients. To the best of our knowledge, the influence of the doping agent itself, without the influence of the doping concentration, has not been examined so far.

In the present study, we report on results during DA at 175 °C and during illumination at different intensities at 75 °C in B- and Ga-doped Cz-Si from the same industrial producer, after having applied the same processes to all wafers (sample preparation and experimental approach are described in Section 5). Both bulk- and surface-related degradation are observed, and both observed to depend strongly on the dopant element.

## 2. Results

2.1. Degradation

2.1.1. Degradation by Carrier Injection

Figure 1 shows the degradation and regeneration of the effective minority charge carrier lifetime of B-doped samples at two different illumination intensities of 0.1 and 1 sun equivalent illumination at a temperature of 75 °C. We refer to these conditions as LeTID treatment. The investigated samples exhibit the expected behavior. The initial lifetime is relatively low due to active BO defects. During the first hours of the LeTID treatment, the lifetime is even further reduced, followed by a steep increase when the regeneration sets in. Both degradation and regeneration are accelerated at higher illumination intensity (i.e., higher excess carrier concentration).[29–33] Note that both LeTID and BO defects regenerate simultaneously (see Section 2.1.2 and 2.4).

The response of the Ga-doped samples to the same conditions is very different, as shown in **Figure 2**. At an illumination intensity equivalent to 1 sun, the carrier lifetime remains relatively stable over time. A minor *dip* might occur at around 1 h of LeTID treatment. By contrast, at an illumination intensity of 0.1 sun
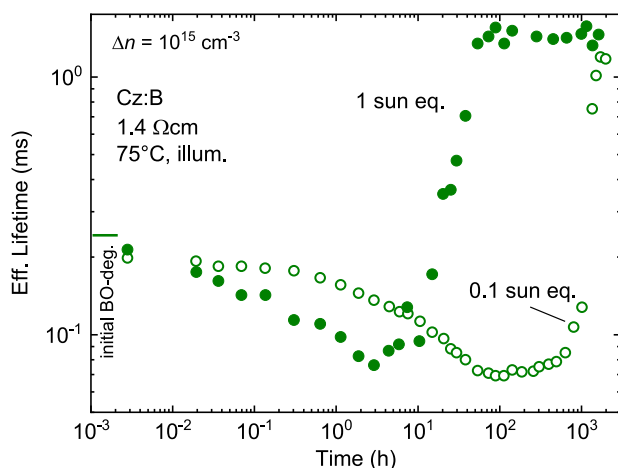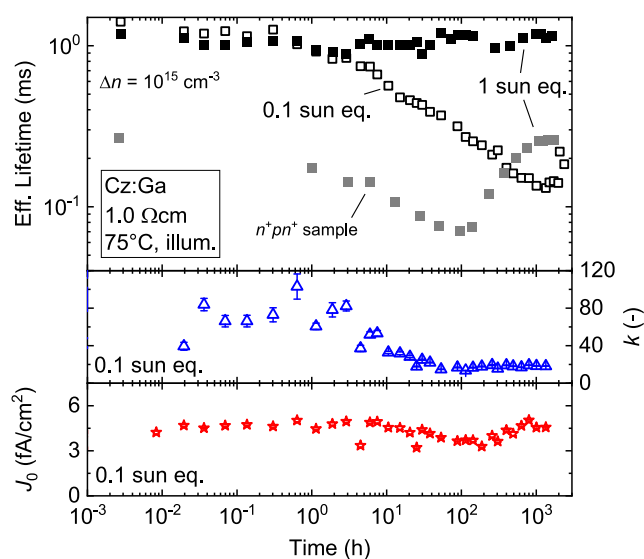
Figure 2. Top: Effective carrier lifetime (evaluated at $\Delta n = 10^{15}$ cm^{-3}) over degradation time of Ga-doped Cz-Si degraded under two different illumination intensities at 75 °C. Open symbols: 0.1 sun eq.; closed symbols: 1 sun eq. illumination intensity. For comparison, one Ga-doped sample with an n$^+$ diffused surface was also degraded at 1 sun eq. (gray rectangles). Center and bottom: Capture cross-sectional ratios k (blue triangles) and surface-related J_0 (red stars) of the Ga-doped sample degraded at 0.1 sun eq., respectively.

equivalent, the carrier lifetime decreases drastically to about 10% of its initial value. As the level of injection seems to be decisive for the degradation extent of the Ga-doped samples, we also subjected a symmetrically P-diffused Cz:Ga sister sample to an illumination at 1 sun eq. at 75 °C (closed gray rectangles in Figure 2). Due to the increased recombination at the diffused surface, the effective lifetime level of this sample is much lower than in the lifetime samples without n$^+$ layer. Indeed, the diffused sample degrades significantly even under 1 sun eq. illumination; it regenerates completely after ≈1000 h treatment time, similar to the Cz:B samples in this study. The sample illuminated at 0.1 sun eq. shows a slight rise in lifetime at the end of the observation period, which might indicate a beginning regeneration.

For better comparison, **Figure 3** plots the normalized lifetime-equivalent defect densities ΔN_{leq} of both B- and Ga-doped samples. This evaluation demonstrates that similar amounts of defects are activated in wafers of both dopant types when they degrade. Note that the smaller relative lifetime change of the Ga-doped sample with diffused surfaces (grey squares) corresponds to significant defect concentrations. It should also be noted that ΔN_{leq} strongly depends on the initial lifetime measurement directly after sample firing. The progression of ΔN_{leq} to negative values indicates that some LeTID defects were already active at the beginning in the boron-doped samples. Interestingly, such a firing-induced initial LeTID defect activation is not observed in the Ga-doped diffused sample, which regains its initial lifetime level.

Figure 2 (bottom) also contains a detailed analysis of the surface-related J_0 of the Ga-doped sample degraded at 0.1 sun eq.

Figure 1. Effective carrier lifetime (evaluated at $\Delta n = 10^{15}$ cm^{-3}) of B-doped Cz-Si in the BO-degraded state over degradation time for two different illumination intensities at 75 °C. Open symbols: 0.1 sun eq.; closed symbols: 1 sun eq. illumination intensity.
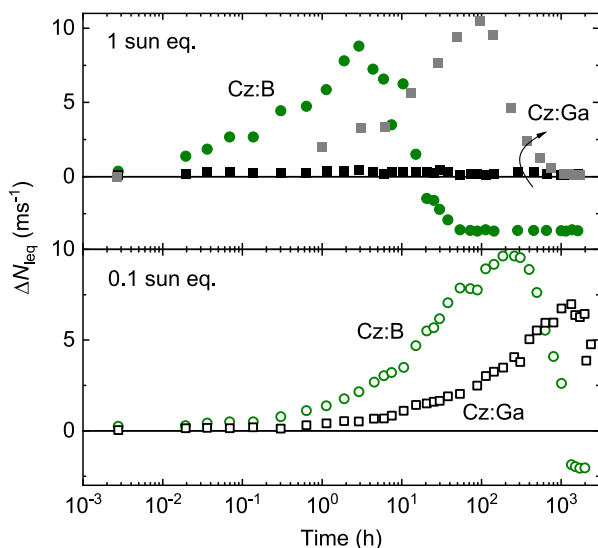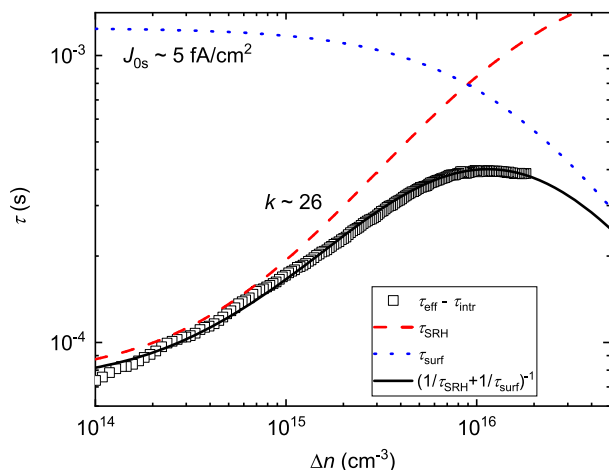
Figure 3. Normalized lifetime-equivalent defect density during degradation at 75 °C and an illumination intensity equivalent to 1 sun (top) and 0.1 sun (bottom) of boron-doped (circles) and Ga-doped (rectangles; black: etched-back, gray: diffused) samples.

Table 1. Degradation rates of the Ga-doped samples during illuminated degradation. As the excess carrier density changes with the carrier lifetime, a range of the estimated density during the treatment is given.

Sample	Illumination	Est. excess carrier den. range [cm]$^{-3}$	Degradation rate [h]$^{-1}$
–/Si:Ga/–	1 sun eq.	8×10^{15}	–
–/Si:B/–		$1-5 \times 10^{15}$	−2.0
n$^+$/Si:Ga/n$^+$		$9 \times 10^{14} - 3 \times 10^{15}$	−0.06
–/Si:Ga/–	0.1 sun eq.	$1 \times 10^{14} - 1 \times 10^{15}$	−0.004
–/Si:B/–		$3 \times 10^{13} - 1 \times 10^{14}$	−0.07

It remains stable at a value around 5 fA cm^{-2} during the entire time, indicating that the observed lifetime changes are due to activation of bulk defects. As shown in Figure 2 (center), the optimum value of the capture cross-sectional ratio k changes with the activation of defects indicated by the reduced effective lifetime. **Figure 4** displays the best fit to the injection-dependent carrier lifetime in the fully degraded state, indicating a k value of ≈26, which is typical for the LeTID defect (for a compilation of literature values, see the previous study[34]). The temporal evolution of the capture cross-sectional ratio indicates the activation of the same or a similar defect as in B-doped mc-Si samples.[35]

For B-doped silicon, a strong correlation between excess carrier concentration and both defect activation (degradation) and
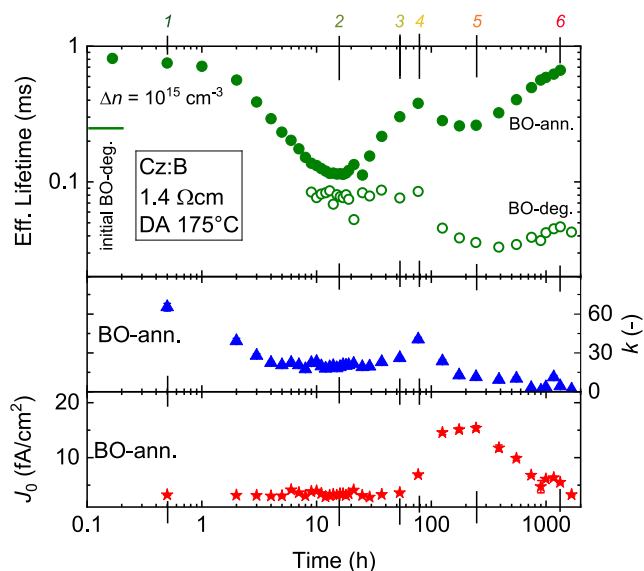
deactivation (regeneration) rate has been established: the higher the injection, the faster the degradation/regeneration cycle proceeds. This trend is again confirmed in the present study; see **Table 1**. It seems to be clear that the degradation and regeneration rates in Ga-doped silicon are, in general, lower than in B-doped material, although a systematic study of the rates in dependence of Δn is still missing. We note that degradation and regeneration are faster in the sample with n$^+$ layers (illuminated with 1 sun eq.) compared with the sample where the diffused region had been etched off (illuminated with 0.1 sun eq.); see Table 1. With our estimated Δn values, these results indicate a similar injection dependence of the rates as in B-doped silicon.

In summary, our results suggest that—although the kinetics and dependence on injections conditions differ—the same defect is activated in both B- and Ga-doped silicon under illumination at elevated temperatures. Reports of a generally lower degradation extent in Ga-doped silicon samples[21] have to be considered with care, as it is important to consider the injection conditions.

2.1.2. Degradation During DA

As observed by Chen et al.,[5] boron-doped samples degrade and regenerate in the dark at intermediate temperatures—in this case 175 °C—in a very similar manner as during illuminated conditions and elevated temperatures. At least, as shown in **Figure 5**, this is the case if the BO defect is in the annealed state (closed symbols) during the lifetime measurement. When we apply a standard BO LID treatment (<0.1 sun eq., room temperature, ≈48 h) before measuring, the carrier lifetime experiences an additional significant reduction as can be expected from the activation of the BO defects (open symbols). Interestingly the BO-degraded carrier lifetime stays constant at a very low level or even suffers an additional decrease while the BO-annealed lifetime is regenerating.

Chen et al. concluded from the degradation and regeneration kinetics as well as from the analysis of the capture cross-sectional ratio that DA activates the same LeTID defect as illumination at lower temperature.[5] Further evidence for this hypothesis comes from the temporal evolution we have observed for k values describing the injection-dependent recombination (see Figure 5, center): again, k values around 20–30 (typical for LeTID) are found during the time range we interpret as maximum LeTID degradation (time range 10–30 h in our experiment).

Figure 4. Analysis of the effective carrier lifetime corrected for the intrinsic recombination (symbols) of the Ga-doped (0.1 sun eq.) sample in the fully degraded state, assuming that the dominating limitations are a single one-level defect and the surface recombination.

Figure 5. Top: Evolution of the effective carrier lifetime during DA at 175 °C of boron-doped samples at fixed injection of $\Delta n = 10^{15}$ cm^{-3}; closed symbols: BO-annealed state, open symbols: BO-degraded state. Center and bottom: Capture cross-sectional ratios k (blue triangles) and surface-related J_0 (red stars), respectively, of the boron-doped samples in the annealed state. The italic numbers on the top refer to the measurement points plotted in Figure 6.
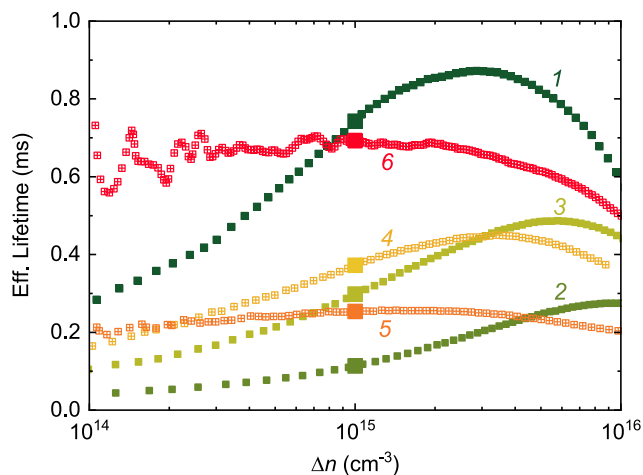

Figure 6. Shift in the injection-dependent carrier lifetime observed during DA of the boron-doped sample. Italic numbers pertain to the points in time as indicated in Figure 5; lifetime values at $\Delta n = 10^{15}$ cm^{-3} are highlighted.

Interestingly, a second dip in both effective lifetime and fitted k factor is observed at about 200 h DA duration, which is accompanied by a distinct shift in the injection dependence of the lifetime. As shown in **Figure 6**, the lifetime at higher injection first decreases, followed by an increase at lower injection, which continues to high lifetime values during regeneration. Assuming that the reduction at high injection is due to surface recombination (see the previous study[28]), the analysis of the surface-related J_0 values (Figure 5, bottom) reveals that this lifetime decrease

is a result of a temporary increase in the surface recombination. During further continuation of the DA treatment, both the surface and the bulk recover, resulting in very high carrier lifetimes with weak injection dependence. Note that a similar analysis in the BO-degraded state was not successful, because the strong bulk recombination interferes with the Kane–Swanson approach.

It seems that at the end of the DA treatment, the LeTID defect is fully recovered while the BO defect can still be activated. Hence, although we cannot discern the regeneration of the BO and the LeTID defect under illumination (see Section 2.4), the regeneration mechanisms, nevertheless, are very different. The very low carrier lifetime in the BO-degraded state even suggests a higher BO defect density after the DA degradation for more than 1000 h.[36] We speculate that this observation is related to reports of excessive LID of B-doped Cz-Si after DA of stabilized PERC solar cells.[37]

Figure 7 (top) displays the carrier lifetime evolution during DA at 175 °C of the Ga-doped sample. The carrier lifetime stays at a constant level for ≈100 h followed by significant degradation. For completeness, we plot values measured after annealing and after BO-degradation treatment (see Figure 5), although they are very similar. We attribute the observed slight differences mainly to a very low Fe contamination. The degradation itself seems to be very dissimilar to the boron-doped samples. When we analyze the injection-dependent lifetime in a similar way as mentioned earlier in terms of a single one-level defect and a surface limitation, the lifetime degradation is not accompanied by changes in J_0. We find that J_0 remains relatively constant at a level of ≈5 fA cm^{-2} (see Figure 7, bottom), which is similar to the result on all other samples in the nondegraded states. This implies the interesting suggestion that the surface-related degradation may depend on the dopant species itself even though both B and Ga are acceptors. During degradation, the injection dependence of
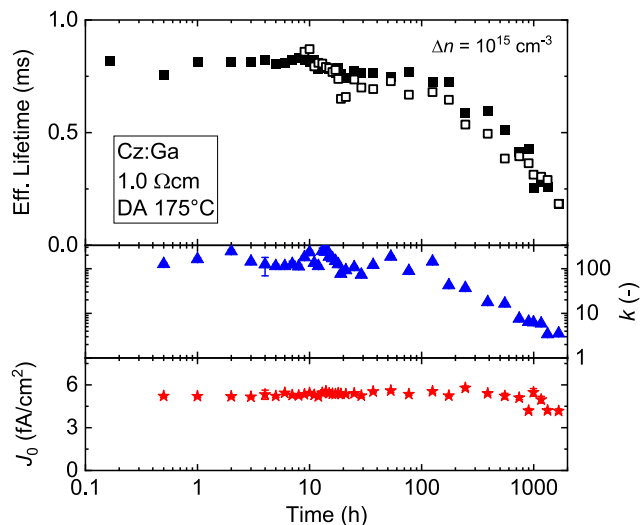
Figure 7. Top: Evolution of the effective carrier lifetime during DA at 175 °C of a gallium-doped sample; closed symbols: BO-annealed state, open symbols: BO-degraded state. Center and bottom: Analysis of the capture cross-sectional ratio k (blue triangles) and J_0 related to the surface (red stars), respectively. Note the different scales compared with Figure 5.
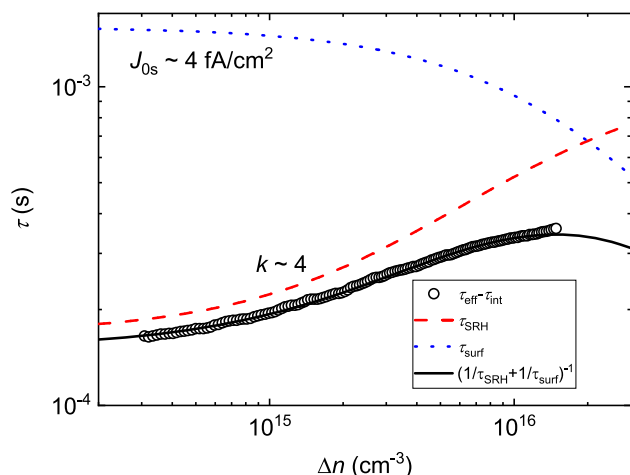
Figure 8. Analysis of the effective carrier lifetime corrected for the intrinsic recombination (symbols) of the Ga-doped sample in the most degraded state after DA, assuming that the dominating limitations are a single one-level defect and the surface recombination.

the carrier lifetime reduces (compare Figure 7, center, and **Figure 8**). The typical fingerprint of $k \sim 20$–30 for the LeTID defect was not observed.

2.2. Temporary Recovery

It is known that the B-doped samples can be degraded and regenerated within seconds at very high injection conditions (obtained, e.g., by laser illumination) and appropriate temperatures.[32] Therefore, the question arises whether the high carrier lifetime in the Ga-doped samples—interrupted only by a slight dip—observed at 1 sun eq. illumination is a result of a comparable, very fast degradation–regeneration cycle, which may have not been recorded with the chosen time resolution. To check this hypothesis, we subjected a Ga-doped sister sample first to 1 sun eq. illumination for 140 h at 75 °C. Again, we observe a slight dip in the carrier lifetime after around $\approx$1 h treatment time (see **Figure 9**). Subsequently, the illumination intensity was reduced to 0.1 sun eq., whereas the temperature was kept constant at 75 °C. The

change in injection conditions resulted in a steep drop in carrier lifetime to the same value and with approximately the same rate as observed on the sample that had been illuminated at 0.1 sun eq. from the beginning. After $\approx$1700 h at 0.1 sun eq., during which only a very slight regeneration can be observed, the sample was again subjected to the higher illumination intensity of 1 sun eq. (T constant at 75 °C). This resulted in a steep increase in carrier lifetime; after $\approx$9 h, almost the initial lifetime level was reached. As a final test, the sample was then again subjected to 0.1 sun eq. for $\approx$300 h (T constant at 75 °C), giving rise to a second significant degradation to almost the same lifetime level as at the end of the first low-intensity degradation step.

A similar TR of the carrier lifetime from the fully degraded state is observed during illumination at lower temperature, such as 25 °C; see **Figure 10**. The samples can be degraded again if subjected to a low illumination at elevated temperature. A thorough discussion of our interpretation of these findings can be found in Section 3.

In contrast to the degradation during illumination at 0.1 sun eq. (Figure 10), we did not observe any TR in the DA-degraded Ga-doped sample upon illumination at 0.5 sun eq. at 25 °C (data not shown). The carrier lifetime stays constant at the same low level even after 1 h of illumination treatment. Both the dissimilar injection dependence in the fully degraded state and the impossibility to temporarily recover the Ga-doped sample after DA could indicate that the LeTID defect is not the cause for the degradation in this case.

2.3. Lateral Appearance

Figure 11 shows the photoluminescence images (PLI) of the temporal evolution during degradation and regeneration of the boron-doped samples, subjected to different degradation conditions, for comparison. It is obvious that carrier injection accelerates the regeneration process to a significant extent: Regeneration starts in the regions with the highest carrier lifetimes (in our case, the upper wafer edge and isolated spots at the right edge where the wafer is in contact with pins of the firing furnace belt). As local lifetime regeneration further increases local excess carrier densities, which diffuse into neighboring regions, the regenerated regions spread. Due to this lateral inhomogeneity, the determination of regeneration rates from quasi-
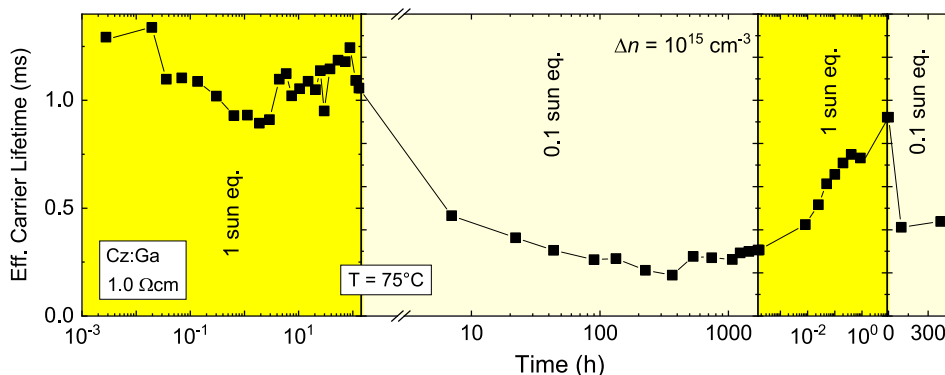

Figure 9. Evolution of the effective carrier lifetime of a Ga-doped sister sample that was alternately illuminated at 1 sun eq. (dark yellow) and 0.1 sun eq. (light yellow) illumination for different periods of time. Note the different timescales. The temperature was kept at 75 °C. The lines are guides to the eye.
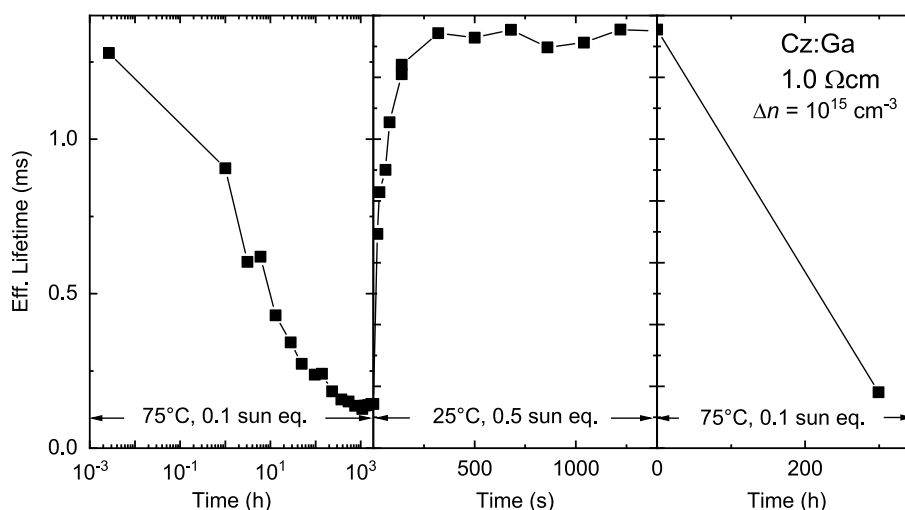
Figure 10. Evolution of the effective carrier lifetime of a Ga-doped sample, subjected first to an illumination of 0.1 sun eq. at 75 °C (left) and subsequently to an illumination of 0.5 sun eq. at 25 °C (right). Note the different timescales. The lines are guides to the eye.
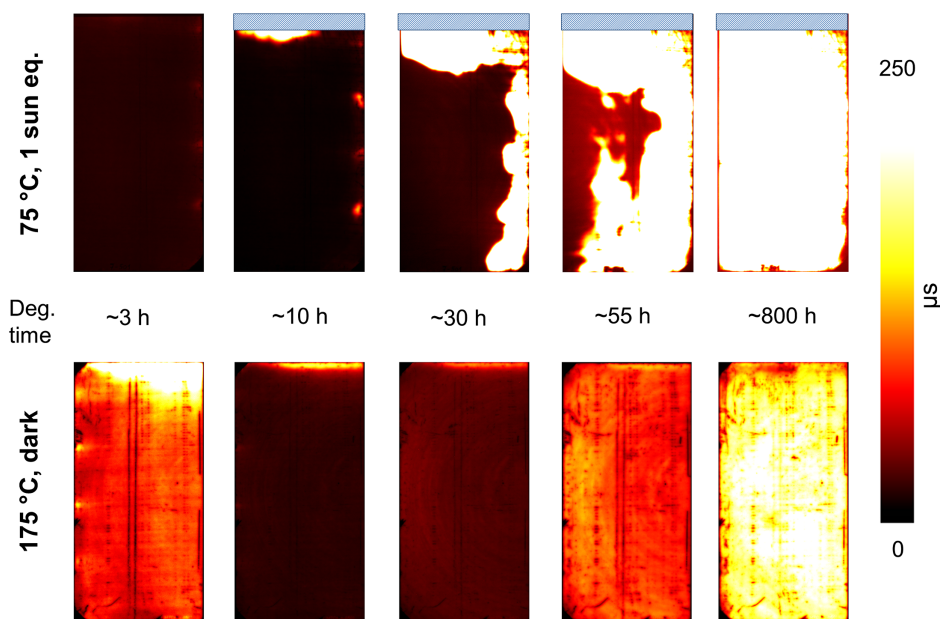
Figure 11. PL images of boron-doped half wafers (obtained at a generation rate of ≈0.1 sun eq. and calibrated to carrier lifetime) during degradation at 75 °C and 1 sun eq. illumination (upper row) and during DA at 175 °C (lower row). The cumulated degradation time steps are indicated in the center row. Note that, to prevent overflow of the camera detector, the upper edge of the LeTID-degraded wafer (upper row) with very high carrier lifetime was masked during the measurement, indicated by the dashed boxes.

steady state photoconductance (QSSPC) measurements has to be considered with precaution.

By contrast, during prolonged dark annealing, the carrier lifetime increases rather homogeneously (aside from local imperfections of the surface passivation).

It is interesting to note that during the LeTID treatment, we cannot discern the regeneration of the BO defect from the same transition of the LeTID defect. Apparently, both processes happen simultaneously. If this was not the case, we would expect to observe a "step-wise" evolution of the carrier lifetime to manifest

in logarithmic plots. Initially, the lifetime becomes limited by quickly activated BO defects, whereas the LeTID defect plays only a minor role. Subsequently, the recombination activity of the latter continually increases until both defects are activated to their maximum. If now the regeneration of one of the defects began while the other stayed active, we would expect an increase in the carrier lifetime until the active defect would dominate. Upon regeneration of the remaining active defect, the carrier lifetime would increase to its maximum. What we observe instead is that the regeneration begins in regions with the highest excess carrier

concentrations (the wafer edges in our case), and the local life-time quickly reaches its final level. At the same time, LeTID degradation is still in progress in the wafer center, indicating that both fully active and completely regenerated BO and LeTID defects are present on the same wafer. This might indicate that the regeneration of both defects is linked to the same underlying process.

During DA, the BO defect is deactivated. As BO regeneration requires BO defects to be in the active state,[38–40] LeTID and BO regeneration are decoupled during DA. This observation suggests that the abovementioned underlying process has a different impact on the two defects.

3. Discussion

The simplest model that can be used to describe most of the observations concerning LeTID is the four-state-model introduced by Fung et al.[41] In the initial stage directly after the firing step, most LeTID defects are found in the recombination-inactive precursor state A. Under degradation conditions, the active LeTID defects form, and the system reaches the degraded state B. Upon prolonged application of the degradation conditions, the recombination-inactive regenerated state C is reached. To account for observations of a resupply of LeTID precursors during DA, a reservoir state R was introduced that can feed into state A. This model was initially developed based on experiments on B-doped substrates and describes their behavior well.

For the case of Ga-doped samples, we think that the general model is still valid: Degradation and regeneration occur, and in the present study, we provide evidence also for the TR. However, the conditions for the transitions between the states differ: Our results suggest that the reaction $B \rightarrow A$, the reverse reaction to degradation, dominates even at elevated temperatures, if the excess carrier concentration exceeds a certain level. As a result, Ga-doped lifetime samples do not degrade if the carrier injection is high in the first place, or they return to state A if they have previously been brought into state B. In other words, in Ga-doped samples, the equilibrium LeTID defect concentration is determined by two parameters, i.e., the temperature and the excess carrier concentration. By contrast, higher injection in boron-doped samples always accelerates the transitions $A \rightarrow B$ and $B \rightarrow C$ if the temperature is above $\approx 50\,°C$. Only below this threshold temperature, the TR transition $B \rightarrow A$ can occur. Hence, in this case, it is the temperature alone, which determines the equilibrium LeTID defect concentration.

Considering the involvement of hydrogen, there are several possible explanations for these observations. First, it is possible that the LeTID precursor/defect includes the dopant element itself, so the LeTID defect would consist of a B–X or Ga–X complex, respectively, with X denoting some unknown components (potentially involving hydrogen). In this case, the LeTID defects would obviously differ on a very basic, direct level when another dopant is used. Both elements exhibiting shallow acceptor levels in the silicon matrix, it is conceivable that both take part in similar complexes—that might impose similar recombination—however, with different binding behavior. Alternatively, the difference in reactions could result from an indirect, secondary effect of the dopants in the complex picture of hydrogen

reactions. It is known that all shallow acceptors form pairs with hydrogen, with some differences in the binding energies.[42] In a previous publication, we hypothesized that during LeTID, the precursor dissociates into the LeTID defect and atomic hydrogen.[43] With the solubility of atomic hydrogen being very low, the degradation can only proceed if the released hydrogen is transferred to a sink, which could be the acceptor atoms. As shown in the previous study,[44] boron–hydrogen pairs dissociate more easily under illumination than in the dark. Zundel et al. explained this by an increased reaction rate of a competing mechanism, the formation of hydrogen molecules, as a result of the increased electron concentration. Hence in this picture, illumination changes the equilibrium distribution between the hydrogen complexes even though the charge carriers are not directly involved in the B–H dissociation. We explained the TR in a very similar manner: under illumination, the hydrogen atoms released from the boron atoms can reform the LeTID precursor, along with hydrogen molecules. We are not aware of a similar investigation of depassivation of Ga acceptors in dependence of excess carrier injection. However, we note that the binding energies (in the dark) between B–H and Ga–H pairs differ (1.28 eV vs 1.40 eV[42]), and that this difference could have an impact on the equilibrium distribution of the hydrogen complexes, including the LeTID defect versus precursor concentrations. It seems contradictory that in Ga-doped samples, where the acceptor–hydrogen pairs appear to be more stable (in the dark), the LeTID defects can be more easily reversed to precursors under illumination. This would indicate excess charge carriers to have a more direct impact on the Ga–H dissociation than expected from the previous study.[44] To resolve this contradiction, the formation and dissociation of Ga–H pairs in the dark and during carrier injection need to be investigated in detail.

According to our observations, the stability of the surface passivation depends on the dopant element of the substrate, as well: while the surface-related J_0 exhibits a significant peak after 100–400 h degradation in the dark for B-doped samples, nothing of the sort happens in the Ga-doped samples despite comparable Fermi-level position. Concurrently, the kinetics of the bulk degradation differ significantly. In a similar investigation to this work, Sperber et al.[45] traced the surface degradation to a temporary loss of the chemical passivation at the interface, i.e., the passivation of the dangling bonds at the Si/AlO_x interface by hydrogen. Again, the different degradation behavior could be a result of the different binding energies of hydrogen to the respective shallow acceptor, which, in turn, has an impact on the hydrogen complex distribution also at the surface.

4. Conclusion

While we can confirm that, under the same illumination conditions, the carrier lifetime of Ga-doped wafers degrades more slowly, the degradation extent significantly depends on the injection conditions. While we observe no significant degradation under 1 sun eq. in the Ga-doped samples, the normalized defect density reaches the same high amount in both materials if a lower injection (≈ 0.1 sun eq., which corresponds better to maximum power point conditions of field application) is applied. We find a carrier cross-sectional ratio k of ≈ 26 in the Ga-doped samples,

which is typical for the LeTID defect. During DA, the B-doped samples first undergo a degradation of the bulk, followed by a surface degradation, which both recover upon prolonged annealing, whereas Ga-doped samples degrade only after an extended period of time, with the cause of degradation being unclear.

This unexpected relation between excess carrier concentration and degradation extent suggests that the dopants themselves are directly involved in the LeTID defect formation mechanism. In addition, the different appearance of the surface degradation could also indicate a dependence on the dopant element. Therefore, repeating experiments that have been conducted on B-doped silicon wafers on Ga-doped samples promises valuable insights into both the LeTID and surface degradation mechanisms.

Beside the scientific importance, the investigation of LeTID on Ga-doped silicon wafers addresses one of the key issues of the photovoltaic industry: ensuring the long-term stability of the modules being currently in mass production.

5. Experimental Section

Material: The Cz-Si wafers used for this experiment were sourced from one industrial producer and consisted of two boron-doped materials (1.6 and 1.4 Ω cm, $[O_i] = 8 \times 10^{17}$ and 5.5×10^{17} cm^{-3}, respectively) and one Ga-doped material (1.0 Ω cm, $[O_i] = 6.5–8 \times 10^{17}$ cm^{-3}). As both B-doped materials exhibit the same trends in all cases, we show only results from the higher doped wafers.

Processing: After saw damage etch and wet chemical cleaning, the wafers underwent an oxidation step at 1050 °C for 80 min followed by an oxide etch, a POCl$_3$ diffusion at 810 °C (60 min., resulting in a sheet resistivity of ~$\approx$100 Ω sq^{-1}). Such high-temperature treatments have been demonstrated to improve the material quality of monocrystalline silicon.[46,47] The diffused region was left intact on several wafers, whereas it was etched off on others, as discussed in the text. Both wafer surfaces were then passivated with a stack of 6 nm Al$_2$O$_3$ (Fast-ALD, Solaytec) and 150 nm SiN$_x$ (PECVD MAiA, Roth&Rau). Finally, the wafers were fast-fired at a measured sample peak temperature of 800 °C. The final thickness of the wafers was 145 ± 4 μm for the etched and 154 ± 4 μm for the diffused samples.

Measurements: The effective minority charge carrier lifetimes (in short addressed as *lifetimes* in this work) were measured ex situ using both harmonically modulated photoluminescence (PL)[48] and a Sinton Instruments WCT-120 lifetime tester (fast flash mode). In addition, PLI were obtained at different generation rates, using laser illumination and a camera with a cooled silicon charge-coupled device. Calibration of the PLI was performed by means of harmonically modulated PL measurements.

Experimental Procedure: The initial measurements were conducted directly after the firing step. Next, the wafers were degraded in ambient light for $\approx$48 h to ensure that all BO-related defects had been formed, and the impact of the metastable iron–acceptor pair dissociation was assessed by the proceeding suggested in the previous study.[49] The Fe content was found to be extremely low and, thus, did not interfere with the significant lifetime changes in this experiment. After these initial tests, the wafers were cut into halves.

Several wafer halves of each material were then degraded in the dark (anneal, DA) at 175 ± 5 °C, and their respective counterparts were degraded under illumination at 75 ± 5 °C with either $\approx$1 or $\approx$0.1 sun eq. white light-emitting diode illumination. While the former treatment transforms the BO defect into the annealed state and does not promote BO regeneration, the latter induces degradation and regeneration of the BO defect running in parallel to LeTID degradation and regeneration. Between the degradation steps, the wafers were repeatedly characterized by QSSPC, harmonically modulated PL and PLI measurements always in the same sequence.

For the DA samples, care was taken to minimize exposure to light between the anneal and the first QSSPC measurement. This gave the carrier lifetime in the BO-annealed, but LeTID-degraded state. After that, injection-dependent PL imaging as well as harmonically modulated PL measurements ensued. Subsequently, the samples were BO-degraded (48 h, ambient light, room temperature) and once again measured by QSSPC to characterize the BO- and LeTID-degraded state. Then, the following DA degradation step ensued. Note that the BO-degradation steps were suspended during the first $\approx$10 h to ensure that the BO-annealed state was kept during the first short DA steps. We are confident that, subsequently, the measurement intervals sufficed for complete transition to the BO-annealed state during DA.

Samples degraded under illumination could not be measured in the BO-annealed state, because the necessary annealing steps at $\approx$200 °C are known to change the LeTID behavior entirely.[32,50,51] Therefore, such wafers were measured only in the fully BO- and LeTID-degraded state.

Some Ga-doped sister samples were tested for TR.[43] This was done in two different ways: 1) The temperature was kept constant at 75 °C, but the illumination conditions were switched between 1 and 0.1 sun eq. intensity. 2) Fully degraded samples were subjected to $\approx$0.5 sun eq. at a "low" temperature of 25 °C. The latter step is known to induce TR in B-doped samples.[33,43]

Analysis: All lifetimes at fixed excess carrier density presented in this work were obtained using harmonically modulated PL. From these, the lifetime-equivalent defect densities ΔN_{leq} were calculated according to

$$\Delta N_{leq}(\Delta n) = \left(\frac{1}{\tau_{eff}(t, \Delta n)} - \frac{1}{\tau_{eff,0}(\Delta n)} \right)^{-1} \quad (1)$$

as suggested by Herguth,[52] with $\tau_{eff,0}$ and τ_{eff} being the effective charge carrier lifetimes directly after firing and at accumulated degradation time t, respectively.

For the determination of the ratio of the electron and hole capture cross sections k and of the surface-related saturation current density J_0, the measured injection-dependent carrier lifetime curves obtained by QSSPC were first corrected for intrinsic recombination using the model by Richter et al. including Auger and radiative recombination.[53,54] The corrected lifetime data were then analyzed in terms of the linearization approach for the Shockley–Read–Hall formalism of Murphy et al.[55] Defects with a single trap level in the bandgap are represented by a linear function. The slope and intercept of the defect fit can then be used to calculate k. The saturation current density J_0 was extracted from the data along with the defect fit by combining the linearization approach and the Kane–Swanson method;[56] details of the applied method will be published in a separate contribution. The measurement uncertainties were calculated by error propagation using the standard errors obtained by the nonlinear fitting algorithm.

Conflict of Interest

The authors declare no conflict of interest.

Data Availability Statement

Research data are not shared.

[1] S. W. Glunz, S. Rein, W. Warta, J. Knobloch, W. Wettling, in *Proc. 2nd World Conference on Photovoltaic Solar Energy Conversion* (Eds: J. Schmid, E.D. Dunlop, H.A. Ossenbrink, P. Helm, H. Ehmann), European Commission, Ispra, Italy **1998**, pp. 1343–1346.

[2] J. Schmidt, *Solid State Phenom.* **2003**, *95–96*, 187.

[3] A. Herguth, G. Schubert, M. Kaes, G. Hahn, in *Proc. 21st European Photovoltaic Solar Energy Conf. and Exhibition* (Ed: J. Poortmans), WIP Renewable Energies, Munich, Germany **2006**, pp. 530–537.

[4] S. W. Glunz, S. Rein, J. Knobloch, W. Wettling, T. Abe, *Prog. Photovolt: Res. Appl.* **1999**, *7*, 463.

[5] D. Chen, M. Kim, B. V. Stefani, B. J. Hallam, M. D. Abbott, C. E. Chan, R. Chen, D. N. Payne, N. Nampalli, A. Ciesla, T. H. Fung, K. Kim, S. R. Wenham, *Sol. Energy Mater. Sol. Cells* **2017**, *172*, 293.

[6] D. Chen, P. G. Hamer, M. Kim, T. H. Fung, G. Bourret-Sicotte, S. Liu, C. E. Chan, A. M. Ciesla née Wenham, R. Chen, M. D. Abbott, B. J. Hallam, S. R. Wenham, *Sol. Energy Mater. Sol. Cells* **2018**, *185*, 174.

[7] C. Renevier, E. Fourmond, M. Forster, S. Parola, M. Le Coz, E. Picard, *Energy Procedia.* **2014**, *55*, 280.

[8] H. C. Sio, H. Wang, Q. Wang, C. Q. Sun, W. Chen, H. Jin, D. Macdonald, *Sol. Energy Mater. Sol. Cells* **2018**, *182*, 98.

[9] K. Ramspeck, S. Zimmermann, H. Nagel, A. Metz, Y. Gassenbauer, B. Birkmann, A. Seidl, in *Proc. 27th European Photovoltaic Solar Energy Conf.* (ED: S. Nowak), WIP Renewable Energies, Munich, Germany **2012**, pp. 861–865.

[10] F. Kersten, P. Engelhart, H.-C. Ploigt, A. Stekolnikov, T. Lindner, F. Stenzel, M. Bartzsch, A. Szpeth, K. Petter, J. Heitmann, J. W. Müller, *Sol. Energy Mater. Sol. Cells* **2015**, *142*, 83.

[11] D. Sperber, A. Heilemann, A. Herguth, G. Hahn, *IEEE J. Photovolt.* **2017**, *7*, 463.

[12] T. Niewelt, F. Schindler, W. Kwapil, R. Eberle, J. Schön, M. C. Schubert, *Prog. Photovolt: Res. Appl.* **2018**, *26*, 533.

[13] D. Chen, P. G. Hamer, M. Kim, C. E. Chan, A. M. Ciesla née Wenham, F. E. Rougieux, Y. Zhang, M. D. Abbott, B. J. Hallam, *Sol. Energy Mater. Sol. Cells* **2020**, *207*, 110353.

[14] D. Bredemeier, D. C. Walter, J. Schmidt, *AIP Conf. Proc.* **2018**, *1999*, 130001.

[15] T. H. Fung, M. Kim, D. Chen, A. Samadi, C. E. Chan, B. J. Hallam, S. Wenham, M. Abbott, *AIP Conf. Proc.* **2018**, *1999*, 130004.

[16] D. Bredemeier, D. Walter, S. Herlufsen, J. Schmidt, *AIP Adv.* **2016**, *6*, 35119.

[17] F. Kersten, J. Heitmann, J. W. Müller, *Energy Proc.* **2016**, *92*, 828.

[18] U. Varshney, M. D. Abbott, A. M. Ciesla née Wenham, D. Chen, S. Liu, C. Sen, M. Kim, S. R. Wenham, B. Hoex, C. E. Chan, *IEEE J. Photovolt.* **2019**, *9*, 601.

[19] C. Sen, C. Chan, P. Hamer, M. Wright, U. Varshney, S. Liu, D. Chen, A. Samadi, A. Ciesla, C. Chong, B. Hallam, M. Abbott, *Sol. Energy Mater. Sol. Cells* **2019**, *200*, 109938.

[20] J. M. Fritz, A. Zuschlag, D. Skorka, A. Schmid, G. Hahn, *Energy Proc.* **2017**, *124*, 718.

[21] N. E. Grant, J. R. Scowcroft, A. I. Pointon, M. Al-Amin, P. P. Altermatt, J. D. Murphy, *Sol. Energy Mater. Sol. Cells.* **2019**, *206*, 110299.

[22] N. E. Grant, P. P. Altermatt, T. Niewelt, R. Post, W. Kwapil, M. C. Schubert, J. D. Murphy, *Sol. RRL* 2000754.

[23] D. Sperber, A. Graf, D. Skorka, A. Herguth, G. Hahn, *IEEE J. Photovolt.* **2017**, *7*, 1627.

[24] D. Sperber, A. Schwarz, A. Herguth, G. Hahn, *Phys. Status Solidi A* **2018**, *215*, 1800741.

[25] T. Niewelt, W. Kwapil, M. Selinger, A. Richter, M. C. Schubert, *IEEE J. Photovolt.* **2017**, *7*, 1197.

[26] T. Niewelt, W. Kwapil, M. Selinger, A. Richter, M. C. Schubert, *Energy Proc.* **2017**, *124*, 146.

[27] D. Sperber, A. Herguth, G. Hahn, *Sol. Energy Mater. Sol. Cells* **2018**, *185*, 277.

[28] D. Sperber, A. Schwarz, A. Herguth, G. Hahn, *Sol. Energy Mater. Sol. Cells* **2018**, *188*, 112.

[29] W. Kwapil, T. Niewelt, M. C. Schubert, *Sol. Energy Mater. Sol. Cells* **2017**, *173*, 80.

[30] S. Liu, C. E. Chan, D. Chen, M. Kim, C. Sen, U. Varshney, B. J. Hallam, M. D. Abbott, S. R. Wenham, D. N. R. Payne, *AIP Conf. Proc.* **2018**, *1999*, 130014.

[31] D. Bredemeier, D. C. Walter, J. Schmidt, *Sol. Energy Mater. Sol. Cells* **2017**, *173*, 2.

[32] C. E. Chan, D. N. R. Payne, B. J. Hallam, M. D. Abbott, T. H. Fung, A. M. Wenham, B. S. Tjahjono, S. R. Wenham, *IEEE J. Photovolt.* **2016**, *6*, 1473.

[33] F. Kersten, P. Engelhart, H.-C. Ploigt, F. Stenzel, K. Petter, T. Lindner, A. Szpeth, M. Bartzsch, A. Stekolnikov, Scherff, M., Heitmann, J., J. W. Müller, in *Proc. 31st European Photovoltaic Solar Energy Conf. and Exhibition* (Eds: S. Rinck, N. Taylor, P. Helm), WIP Renewable Energies, Munich, Germany **2015**, pp. 1830–1834.

[34] D. Chen, M. Vaqueiro Contreras, A. Ciesla, P. Hamer, B. Hallam, M. Abbott, C. Chan, *Prog. Photovolt: Res. Appl.*, *29*, 3.

[35] M. A. Jensen, A. E. Morishige, J. Hofstetter, D. B. Needleman, T. Buonassisi, *IEEE J. Photovolt.* **2017**, *7*, 980.

[36] D. C. Walter, R. Falster, V. V. Voronkov, J. Schmidt, *Sol. Energy Mater. Sol. Cells* **2017**, *173*, 33.

[37] F. Fertig, R. Lantzsch, F. Frühauf, F. Kersten, M. Schütze, C. Taubitz, J. Lindroos, J. W. Müller, *Sol. Energy Mater. Sol. Cells* **2019**, *200*, 109968.

[38] P. Hamer, B. Hallam, M. Abbott, C. Chan, N. Nampalli, S. Wenham, *Sol. Energy Mater. Sol. Cells* **2016**, *145*, 440.

[39] B. Hallam, M. Abbott, N. Nampalli, P. Hamer, S. Wenham, *J. Appl. Phys.* **2016**, *119*, 65701.

[40] B. Hallam, A. Herguth, P. Hamer, N. Nampalli, S. Wilking, M. Abbott, S. Wenham, G. Hahn, *Appl. Sci.* **2018**, *8*, 10.

[41] T. H. Fung, M. Kim, D. Chen, C. E. Chan, B. J. Hallam, R. Chen, D. N. R. Payne, A. M. Ciesla née Wenham, S. R. Wenham, M. D. Abbott, *Sol. Energy Mater. Sol. Cells* **2018**, *184*, 48.

[42] T. Zundel, J. Weber, *Phys. Rev. B.* **1989**, *39*, 13549.

[43] W. Kwapil, J. Schon, T. Niewelt, M. C. Schubert, *IEEE J. Photovolt.* **2020**, *10*, 1591.

[44] T. Zundel, J. Weber, *Phys. Rev. B.* **1991**, *43*, 4361.

[45] D. Sperber, A. Herguth, G. Hahn, *Energy Proc.* **2016**, *92*, 211.

[46] T. Niewelt, A. Richter, T. C. Kho, N. E. Grant, R. S. Bonilla, B. Steinhauser, J.-I. Polzin, F. Feldmann, M. Hermle, J. D. Murphy, S. P. Phang, W. Kwapil, M. C. Schubert, *Sol. Energy Mater. Sol. Cells* **2018**, *185*, 252.

[47] B. A. Veith-Wolf, S. Schäfer, R. Brendel, J. Schmidt, *Sol. Energy Mater. Sol. Cells* **2018**, *186*, 194.

[48] J. A. Giesecke, M. C. Schubert, B. Michl, F. Schindler, W. Warta, *Sol. Energy Mater. Sol. Cells* **2011**, *95*, 1011.

[49] M. C. Schubert, H. Habenicht, W. Warta, *IEEE J. Photovolt.* **2011**, *1*, 168.

[50] C. Chan, T. H. Fung, M. Abbott, D. Payne, A. Wenham, B. Hallam, R. Chen, S. Wenham, *Sol. RRL* **2017**, *1*, 1600028.

[51] T. Luka, M. Turek, C. Hagendorf, *Sol. Energy Mater. Sol. Cells* **2018**, *187*, 194.

[52] A. Herguth, *IEEE J. Photovolt.* **2019**, *9*, 1182.

[53] A. Richter, S. W. Glunz, F. Werner, J. Schmidt, A. Cuevas, *Phys. Rev. B.* **2012**, *86*, 165202.

[54] T. Trupke, M. A. Green, P. Würfel, P. P. Altermatt, A. Wang, J. Zhao, R. Corkish, *J. Appl. Phys.* **2003**, *94*, 4930.

[55] J. D. Murphy, K. Bothe, R. Krain, V. V. Voronkov, R. J. Falster, *J. Appl. Phys.* **2012**, *111*, 113709.

[56] D. E. Kane, R. M. Swanson, in *Proc. 18th IEEE Photovoltaic Specialists Conf.*, IEEE, New York, NY, USA **1985**, pp. 578–583.